Please cite this paper as:

Cai Q, Chen ZW, Zhu S and Mo LY. (2022). On damage detection of beam structures using multiple types of influence lines. Structures. 42: 449-465.

https://doi.org/10.1016/j.istruc.2022.06.022

On Damage Detection of Beam Structures using Multiple Types of Influence Lines

Qin-Lin CAI[1,2], Zhi-Wei CHEN[2], Songye ZHU[1,*], Lu-Ye MO[2]

1. Department of Civil and Environmental Engineering, The Hong Kong Polytechnic University, Hong Kong, China

2. Department of Civil Engineering, Xiamen University, Xiamen, China

* Corresponding author: Prof. Songye ZHU, M.ASCE, Email: songye.zhu@polyu.edu.hk

Abstract

Damage indices that are sensitive to early damage or abnormality of bridges are essential to take protective measures before any catastrophic failure of bridges occurs. Influence lines (ILs) have been proved as a promising bridge damage index numerically and experimentally. However, a comprehensive study on using various types of ILs for damage detection is still unavailable. This paper explicitly reveals the intrinsic relationships among various types of ILs, including deflection, rotation, bending stress, and shear stress ILs, and their corresponding first- and second-order finite differences with respect to moving force locations. Subsequently, the sensitivities and detectable ranges of various types of ILs are investigated and compared systematically through two representative examples, namely, a simply supported beam and a continuous beam. The sensor locations that correspond to high sensitivities and wide detectable ranges are identified for various types of ILs. The pros and cons of calculating the finite differences of ILs for damage detection are also illustrated with consideration of measurement noise. An experiment on a simply supported beam was conducted to partially validate the findings in this study. The conclusions of this study answer fundamental questions regarding the rational selections of IL types and sensor locations in IL-based damage detection methods.

Keyword: sensitivity analysis; influence line; damage detection; bridge health monitoring

1 Introduction

The long-term effects of traffic loads and harsh environmental conditions cause the continuous deterioration and damage accumulation of bridges during their long service life. Bridge monitoring systems that adopt various types of sensors have been extensively deployed recently, and different techniques based on sensing data were developed for load characterization, system identification, or abnormality detection of bridges [1-3]. Vibration-based damage detection methods are regarded as best-known groups that can be categorized into two sub-groups, namely, frequency- and time-domain methods [4-6]. The family of frequency-domain methods includes, but is not limited to, those based on change in frequencies [7], mode shapes [8], frequency response functions [9], mode shape curvature [10], and modal strain energy [11]. Although they demonstrated varying degrees of success in previous studies, these dynamic characteristics (e.g., modal frequencies) or responses are either insensitive to local damage or too sensitive to changes in ambient environment (e.g., temperature) [12]. Among the time-domain methods, representative examples correspond to those employing moving load-induced response time histories [13-16]. The merits of the moving load-based methods are: they closely resemble the actual conditions of vehicles passing a bridge; they can excite structures with large amplitudes and high signal-to-noise ratios when moving loads get close to sensor locations [17]; and they require relatively fewer sensors when applied in large-scale bridges [18].

Meanwhile, influence lines (ILs), which are in close proximity to slowly moving load-induced responses and represent static properties that describe the variation of reactions, internal loadings, displacements, or stresses at specific locations, have been widely adopted in various bridge engineering applications, such as bridge design and performance evaluation [19,20], bridge weight-in-motion [21], and model updating [22,23]. The IL-based methods show their superiority in mitigating the impact of temperature fluctuations and zero drift because the measurement duration is considerably shorter than the environmental change period [12]. Very recently, IL-based damage detection approaches have emerged. For example, Zaurin and Catbas [24] identified the strain ILs of a four-span bridge model by integrating video images and sensor data and then verified that it was a promising damage indicator experimentally [25]. Later, the methodology was applied to detect and locate common damage scenarios on a steel bascule bridge [26]. Chen et al. [12] proposed a group of stress IL (SIL)-based damage localization indices and verified its effectiveness through a case study of Tsing Ma Bridge, in which the damage-induced SIL change ratio at the measured location was approximately 10%–20%, considerably higher than the frequency change ratio. Considering the environmental and measurement noise in sensor data, Zhu et al. [27] further integrated multiple SILs with information fusion technique to improve the accuracy of damage localization. More recently, Chen et al. [28] investigated and verified a deflection IL (DIL)-based damage quantification method for beam structures experimentally. The recorded maximum DIL change ratio was 13% of the amplitude of the baseline DILs, whereas the frequency change ratio was only 1.8%. Zeinail and Story [29] proposed a damage localization and quantification method based on the second-derivative of DIL. Alamdari et al. [30] explored a damage identification technique based on rotation ILs (RILs) for a cable-stay bridge. Huseynov et al. [31] adopted the RIL difference between healthy and damaged states as a damage indicator and located the damage location successfully in the experiment of a simply supported beam. The sensitivity of RIL to damage was also briefly discussed based on the experimental results. More studies about IL-based damage detection approaches include, but are not limited to, those reported in [32-35]. Numerical case studies, laboratory experiments, and even field tests have been conducted in the aforementioned studies and demonstrated the prospect of IL-based damage detection methods in comparison with frequency change ratios. Meanwhile, numerous studies have verified the feasibility of ILs extraction from the moving vehicle-induced dynamic responses of a bridge by using various algorithms [12,36-39]. More detailed information on bridge IL identification has been summarized in the review [40].

A series of past studies proved that ILs were promising and effective damage indices for bridge structures, in which different structural topologies, damage scenarios, and ILs types (including finite differences of ILs) were considered. However, several fundamental issues, such as the intrinsic relationships, sensitivities, and detectable ranges of various ILs, have failed in drawing adequate attention. The insightful answers based on parallel comparisons will be essential for the selection of appropriate IL indices, optimal sensor placement, and condition assessment of beam structures using ILs.

To this end, this paper presents a systematic study on the damage detection of beam structures using various types of ILs and their finite differences. First, in a simply supported beam example, the analytical expression of damage-induced DIL changes and partial derivatives of DIL changes with respect to force and sensor locations are presented, where the intrinsic relationships among various types of ILs are revealed. Subsequently, a numerical example of a three-span continuous beam is established to analyze and compare the damage sensitivities of various ILs of interest and their corresponding finite differences in a dimensionless way. The noise effect on the detection performance of IL-based indices is also discussed briefly in this section. Then, the detectable range of various ILs from different sensor locations is evaluated, thereby shedding light on optimal sensor selection and placement. Finally, an experiment on a simply supported beam was conducted to validate parts of the findings in the study.

Unlike the past studies in which various types of IL-based indices were adopted intuitively, this work aims to: (1) reveal the intrinsic relationships among different IL-based indices, including different types of ILs and their finite differences; (2) systematically compare different IL-based indices in beam structures in terms of damage sensitivity and anti-noise performance; (3) shed light on the multi-type sensor placement and rational selection of IL-based indices for different beam configurations; and (4) experimentally validate the feasibility and effectiveness of the first-order finite difference of IL changes in damage localization.

2 Relationship of Various ILs

As mentioned previously, the use of various ILs, including DIL, RIL, and SIL, have been proposed for damage detection in beam structures [12,30,31]. A general concept is to use the change in ILs as an effective indicator of beam damage:

$$\Delta \mathrm{IL} = \mathrm{IL}_{\mathrm{d}} - \mathrm{IL}_{\mathrm{u}}, \tag{1}$$

where the subscripts u and d stand for the undamaged and damaged statuses, respectively. In addition to the direct use of the IL change, the finite difference of different orders was also suggested to construct improved damage indices [12].

This section illustrates the impact of damage on different types of ILs and the relationships among different types of IL-based indices by using a damaged simply supported beam. The example of a simply supported beam is selected because: (a) its ILs can be derived mathematically, thereby enabling analytical discussions; and (b) it represents a simple and common form of bridges, covering approximately 95% of the recently-constructed high-speed rail bridges in China [41]. A more complicated three-span continuous beam will be analyzed numerically in the next section.

Fig. 1 shows the schematic of a damaged simply supported beam subjected to a moving load, where l is the beam length; EI is the flexural rigidity of the cross section; x is the position of the moving load; y is the sensor location; and c and 2ξ express the location and extent of the damaged elements, respectively.

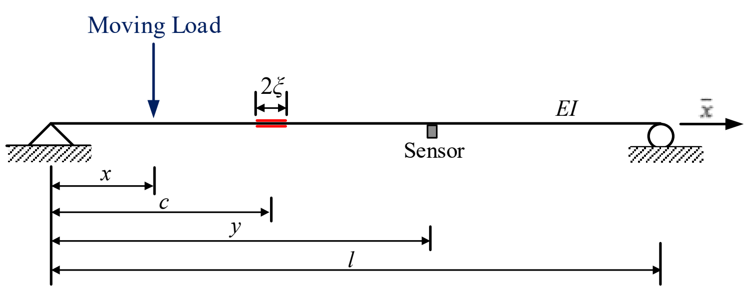

Fig. 1 Simply supported beam under a moving load.

2.1 Damage-induced DIL Change

Among various types of ILs, DIL has very straightforward physical meaning. The deflection under a unit load represents the beam's flexibility. Thus, a DIL under a moving load represents a row or subrow in the flexibility matrix of the beam, and multiple DILs represent a submatrix of the flexibility matrix [12,28]. However, compared with a finite number of elements in the flexibility matrix, DILs represent curves with much higher spatial resolution. Consequently, any structural stiffness loss caused by local damage or global deterioration changes DILs. DIL changes can be monitored at different stages to evaluate the performance of a bridge in its life cycle.

When a unit load is located at position *x*, the deflection of the intact beam measured by a displacement sensor at position *y* can be derived mathematically by using the diagram multiplication method,

$$\mathrm{DIL}(x,y)=\frac{1}{EI}\begin{cases}\dfrac{-(l-y)\left(y^2-2ly+x^2\right)x}{6l} & 0\le x\le y\\[2ex] \dfrac{-(l-x)\left(y^2-2lx+x^2\right)y}{6l} & y\le x\le l\end{cases},\tag{2}$$

where flexural rigidity *EI* is assumed uniform along the intact beam.

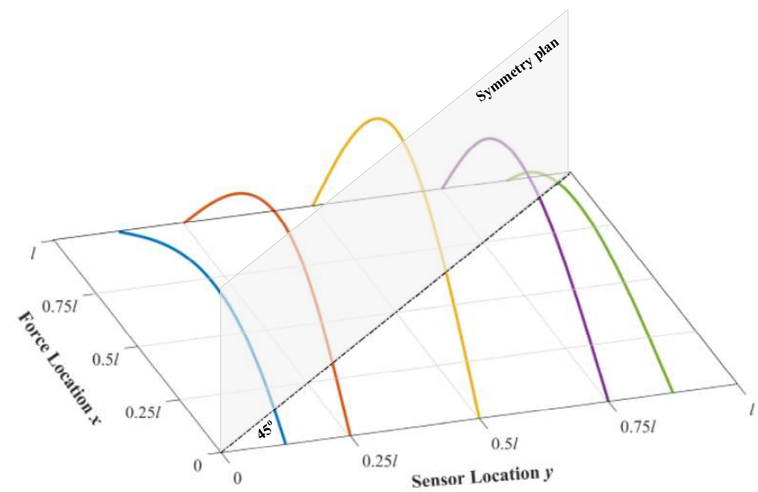

Fig. 2 Multiple DILs form a deflection influence surface.

Given a fixed sensor location y_i, varying *x* value in Eq. (2) provides a DIL function/curve. When multiple displacement sensors are installed at different locations (Fig. 2), connecting multiple DILs forms an unusual influence surface defined by Eq. (2). Notably, the definition of influence surface herein refers to Eq. (2) for a beam and is different from the traditional concept that corresponds to three-dimensional (3D) structures. The deflection influence surface DIL(*x*, *y*) possesses the following features:

(1) According to Maxwell's theorem of reciprocal displacements, DIL(*a*, *b*) = DIL(*b*, *a*). Thus, the deflection influence surface is symmetrical about the 45° line. This property of symmetry is applicable to any types of beam structures, including a damaged beam;

(2) Given a limited number of sensors and the high sampling frequency of each sensor, the spatial resolutions of the influence surface vary. Thus, high resolution in the *x*-direction and low resolution in the *y*-direction can be achieved.

If a damage occurs in the segment [$c - \xi$, $c + \xi$] where the flexural rigidity reduces to $EI_{\mathrm{d}} = (1-\alpha)EI$, then the corresponding DIL change (i.e., ΔDIL) induced by the damage is given by,

$$\Delta\mathrm{DIL}(x,y) = \frac{\alpha}{(1-\alpha)EI}\int_{c-\xi}^{c+\xi} M_{\mathrm{y}}(\bar{x},y) M_{\mathrm{m}}(\bar{x},x) d\bar{x}\,, \tag{3}$$

where α is the damage coefficient; and $M_{\mathrm{m}}(\bar{x},x)$ and $M_{\mathrm{y}}(\bar{x},y)$ denote the bending moment functions at an arbitrary location $\bar{x}$ along the beam when a unit vertical force acts at locations x and y, respectively. Notably, the simply supported beam is a statically determinate structure, and thus the bending moment functions $M_{\mathrm{m}}(\bar{x},x)$ and $M_{\mathrm{y}}(\bar{x},y)$ does not change before and after damage. The flexural rigidity only changes in the damaged segment [$c - \xi$, $c + \xi$]. Therefore, only the integral interval [$c - \xi$, $c + \xi$] needs to be considered in the above equation.

Specifically, if the damage is located at the left side of the sensor location (i.e., $c + \xi < y$), then the DIL change ΔDIL in a simply supported beam can be expressed as

$$\Delta\mathrm{DIL}(x,y) = \frac{\alpha}{(1-\alpha)EI}\begin{cases} \dfrac{2\xi(l-y)\left(3lc-3c^2-\xi^2\right)x}{3l^2} & 0 \le x \le c-\xi \\ \dfrac{-(l-y)}{6l^2}\left\{ lx^3 + x\begin{bmatrix} 4\left(\xi^3+3\xi c^2\right) \\ -3l(c+\xi)^2 \end{bmatrix} + 2l(c-\xi)^3 \right\} & c-\xi \le x \le c+\xi \\ \dfrac{2\xi(l-y)\left(\xi^2+3c^2\right)(l-x)}{3l^2} & c+\xi \le x \le l \end{cases}. \tag{4}$$

Similarly, if the damage is located at the right side of the sensor location (i.e., $c - \xi > y$), then ΔDIL is given as

$$\Delta\mathrm{DIL}(x,y) = \frac{\alpha}{(1-\alpha)EI}\begin{cases} \dfrac{2y\xi\left(3l^2-6lc+3c^2+\xi^2\right)x}{3l^2} & 0 \le x \le c-\xi \\ \dfrac{y}{6l^2}\left\{\begin{matrix} lx^3 - 3l^2x^2 + x\begin{bmatrix} 4\left(\xi^3+3\xi c^2\right) \\ +6l^2(c+\xi) \\ -3l\left(c^2+\xi^2+6c\xi\right) \end{bmatrix} \\ +2l(c-\xi)^3 - 3l^2(c-\xi)^2 \end{matrix}\right\} & c-\xi \le x \le c+\xi \\ \dfrac{2y\xi\left(3lc-\xi^2-3c^2\right)(l-x)}{3l^2} & c+\xi \le x \le l \end{cases}. \tag{5}$$

Fig. 3 shows the change in the deflection influence surface ΔDIL(x, y) induced by a damage located at $c = 0.3375l$ with damage severity $\alpha = 0.05$ and extent $2\xi = l/120$ in the simply supported beam. Given that the influence surfaces of the simply supported beam with and without damage are both symmetrical about the 45° diagonal line, Fig. 3 shows that the damage-induced change ΔDIL(x, y) is also symmetrical about the same line. In Eqs. (4) and (5), given a sensor location y_i and a damage location c, the DIL change ΔDIL is a linear function of the force location x with positive and negative slopes on the two sides of the damage. This phenomenon explains why the peak of any ΔDIL(x, y_i) in Fig. 3 can be an indicator of damage location, regardless of where the displacement sensor y_i is located. Moreover, Fig. 3 illustrates that the ΔDIL change becomes more significant (i.e., more sensitive to the damage) when the displacement sensor comes closer to the damage location; meanwhile, the change ΔDIL will be minimal if the damage location is far from the measurement location of DIL.

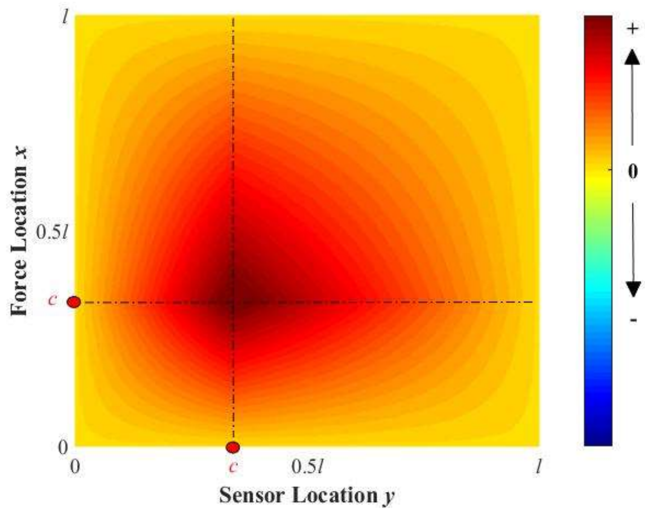

Fig. 3 Change ΔDIL(x, y) induced by a damage at c = 0.3375l in a simply supported beam.

2.2 Other Types of ILs

Chen et al. [12] suggested to calculate the finite difference of the change in ILs as new damage indices with improved sensitivity. If the DIL is measured with a high spatial resolution in the x-direction (i.e., with high sampling rate in comparison with moving speed of the unit force), then the first- and second-order difference terms approximate the derivatives with respect to the force location x,

$$\frac{\Delta\mathrm{DIL}\left(x+\Delta x, y\right)-\Delta\mathrm{DIL}\left(x, y\right)}{\Delta x} \approx \frac{\partial \Delta\mathrm{DIL}\left(x, y\right)}{\partial x} = \Delta\mathrm{DIL}\left(x, y\right)_{,x}, \tag{6}$$

$$\frac{\Delta\mathrm{DIL}\left(x+\Delta x, y\right)-2\Delta\mathrm{DIL}\left(x, y\right)+\Delta\mathrm{DIL}\left(x-\Delta x, y\right)}{\left(\Delta x\right)^2} \approx \frac{\partial^2 \Delta\mathrm{DIL}\left(x, y\right)}{\partial x^2} = \Delta\mathrm{DIL}\left(x, y\right)_{,xx}. \tag{7}$$

Given the typically low density of sensors, calculating the derivatives of ΔDIL(x, y) directly with respect to the sensor location y is difficult. However, based on the relationships among deflection, rotation, bending moment, and shear force of a beam, the changes in RIL, bending moment IL, and shear force IL can be expressed as the equivalent derivatives with respect to y location

$$\Delta\mathrm{RIL}(x,y)=\frac{\partial\Delta\mathrm{DIL}(x,y)}{\partial y}=\Delta\mathrm{DIL}(x,y)_{,y}\,, \tag{8}$$

$$\Delta\mathrm{MIL}(x,y)=\begin{cases}EI(y)\cdot\mathrm{DIL_u}(x,y)_{,yy}-EI_\mathrm{d}(y)\cdot\mathrm{DIL_d}(x,y)_{,yy} & \text{if } c-\xi\le y\le c+\xi\\ -EI(y)\cdot\Delta\mathrm{DIL}(x,y)_{,yy} & \text{otherwise}\end{cases}, \tag{9}$$

$$\Delta\mathrm{FIL}(x,y)=\begin{cases}EI(y)\cdot\mathrm{DIL_u}(x,y)_{,yyy}-EI_\mathrm{d}(y)\cdot\mathrm{DIL_d}(x,y)_{,yyy} & \text{if } c-\xi\le y\le c+\xi\\ -EI(y)\cdot\Delta\mathrm{DIL}(x,y)_{,yyy} & \text{otherwise}\end{cases}, \tag{10}$$

where ΔRIL, ΔMIL, and ΔFIL denote the changes in the RIL, bending moment IL, and shear force IL, respectively. In practice, bending and shear stress ILs of the beam are more often measured to estimate bending moment and shear force, respectively. The corresponding IL changes are given as

$$\Delta\mathrm{BSIL}(x,y)=\begin{cases}\dfrac{EI(y)}{W_\mathrm{u}(y)}\cdot\mathrm{DIL_u}(x,y)_{,yy}-\dfrac{EI_\mathrm{d}(y)}{W_\mathrm{d}(y)}\cdot\mathrm{DIL_d}(x,y)_{,yy} & \text{if } c-\xi\le y\le c+\xi\\ -\dfrac{EI(y)}{W_\mathrm{u}(y)}\cdot\Delta\mathrm{DIL}(x,y)_{,yy} & \text{otherwise}\end{cases}, \tag{11}$$

$$\Delta\mathrm{SSIL}(x,y)=\begin{cases}\dfrac{EQ_\mathrm{u}(y)}{t_\mathrm{u}(y)}\cdot\mathrm{DIL_u}(x,y)_{,yyy}-\dfrac{EQ_\mathrm{d}(y)}{t_\mathrm{d}(y)}\cdot\mathrm{DIL_d}(x,y)_{,yyy} & \text{if } c-\xi\le y\le c+\xi\\ -\dfrac{EQ_\mathrm{u}(y)}{t_\mathrm{u}(y)}\cdot\Delta\mathrm{DIL}(x,y)_{,yyy} & \text{otherwise}\end{cases}, \tag{12}$$

where ΔBSIL and ΔSSIL stand for the change in the bending and shear stress ILs, respectively; W is the section modulus to calculate critical bending stress; and Q and t are the first moment of area (static moment) and cross-sectional width used to calculate critical shear stress, respectively. The bending and shear stresses herein refer to the maximum stresses of a section.

Given ΔDIL in Eq. (4), Eqs. (8)–(12) can be rewritten as

$$\Delta\mathrm{RIL}(x,y)=\frac{\alpha}{(1-\alpha)EI}\begin{cases}\dfrac{-2\xi\left(3lc-3c^2-\xi^2\right)x}{3l} & 0\le x\le c-\xi\\ \dfrac{1}{6l^2}\left\{lx^3+x\begin{bmatrix}4\left(\xi^3+3\xi c^2\right)\\ -3l(c+\xi)^2\end{bmatrix}+2l(c-\xi)^3\right\} & c-\xi\le x\le c+\xi\\ \dfrac{-2\xi\left(\xi^2+3c^2\right)(l-x)}{3l^2} & c+\xi\le x\le l\end{cases}, \tag{13}$$

$$\Delta\mathrm{MIL}(x,y)=0\,, \tag{14}$$

$$\Delta\mathrm{FIL}(x,y)=0\,, \tag{15}$$

$$\Delta\mathrm{BSIL}(x,y)=\begin{cases}\left(\dfrac{1}{W_\mathrm{u}(y)}-\dfrac{1}{W_\mathrm{d}(y)}\right)EI(y)\cdot\mathrm{DIL_u}(x,y)_{,yy} & \text{if } c-\xi\le y\le c+\xi\\ 0 & \text{otherwise}\end{cases}, \tag{16}$$

$$\Delta\mathrm{SSIL}\left(x,y\right)=\begin{cases}\left(\dfrac{Q_{\mathrm{u}}\left(y\right)}{I_{\mathrm{u}}\left(y\right)t_{\mathrm{u}}\left(y\right)}-\dfrac{Q_{\mathrm{d}}\left(y\right)}{I_{\mathrm{d}}\left(y\right)t_{\mathrm{d}}\left(y\right)}\right)EI\left(y\right)\cdot\mathrm{DIL}_{\mathrm{u}}\left(x,y\right)_{,yyy} & \text{if } c-\xi\le y\le c+\xi \\ 0 & \text{otherwise}\end{cases}. \tag{17}$$

Eqs. (6)–(12) lead to an interesting conclusion that various types of IL changes are related to the partial derivatives of ΔDIL of different orders and with respect to various variables. Therefore, the discussion of ΔDIL and their partial derivatives will shed light on the damage effect on various ILs. Notably, Eq. (13) only corresponds to the ΔRIL measured at the right side of the damage location (i.e., $c+\xi<y$).

Fig. 4 shows different partial derivatives of the deflection influence surface change induced by a damage located at c = 0.3375l. The following findings and discussions can be made after the inspections of Eqs. (6)–(17) and Fig. 4:

Considering the symmetry of ΔDIL surface, calculating the partial derivatives of the symmetric ΔDIL surface with respect to the x or y dimension produces similar effects. Therefore, $\Delta\mathrm{DIL}_{,yx}$ and $\Delta\mathrm{DIL}_{,yyxx}$ in Fig. 4 are also symmetrical surfaces about the 45° diagonal line, whereas other surfaces are no longer symmetrical.

For the same reason, the pairs $\Delta\mathrm{DIL}_{,x}$ and $\Delta\mathrm{DIL}_{,y}$, $\Delta\mathrm{DIL}_{,xx}$ and $\Delta\mathrm{DIL}_{,yy}$, and $\Delta\mathrm{DIL}_{,yxx}$, and $\Delta\mathrm{DIL}_{,yyx}$ in Fig. 4 are mirror-symmetrical to each other. This phenomenon reveals the intrinsic relationships between the first-order difference of deflection $\Delta\mathrm{DIL}_{,x}$ and the rotation ΔRIL (Eq. (13)), and between the second-order difference of deflection $\Delta\mathrm{DIL}_{,xx}$ and the bending stress ΔBSIL (Eq. (16)). The corresponding surface changes are similar in terms of magnitude and trend. However, it does not mean that their corresponding ILs will be the same. In fact, they represent the observations of the same surface in different directions. For example, the IL change curves $\Delta\mathrm{DIL}_{,x}$ and ΔRIL can be obtained by cutting the influence surface in Fig. 4(b) in the y- and x-directions, respectively. Fig. 5 shows the representative IL changes at selected locations, y = 0.2l, 0.5l, and 0.75l.

The ΔDIL function shown in Eq. (4) is derivable. However, the partial derivative results change dramatically in the damaged segment, which results in the discontinuity in the partial derivatives on two sides of the damaged segments (Fig. 5(b)). Such discontinuity can be utilized to identify damage locations that can be more than one. For example, $\Delta\mathrm{DIL}_{,x}$ in the undamaged segments are constant, and thus the damage location can be identified via either a sudden drop or rise in the magnitude.

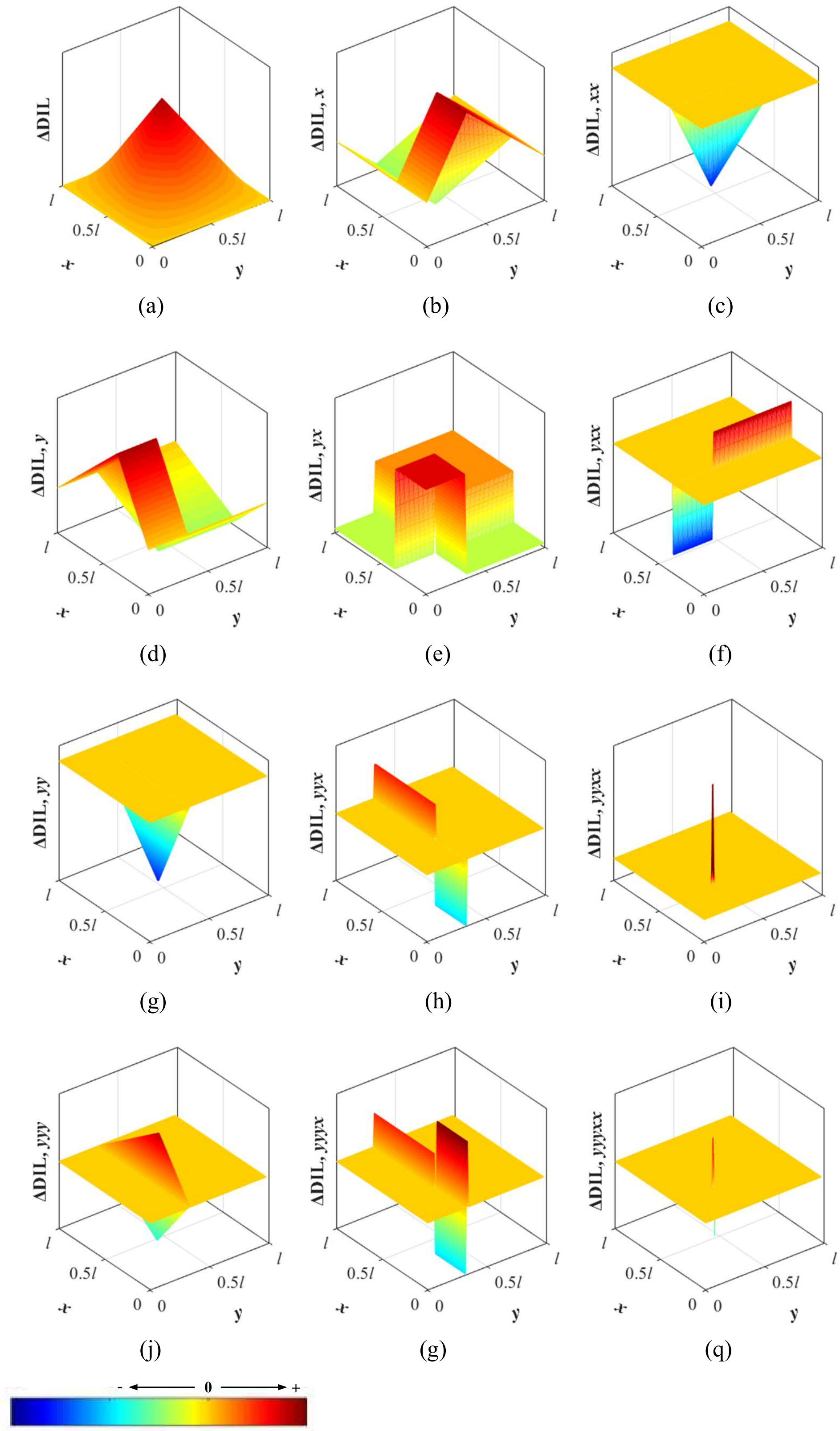

Fig. 4 Partial derivatives of the deflection influence surface change ΔDIL induced by a damage at $c = 0.3375l$ in the simply supported beam (x and y are the force and sensor locations, respectively).

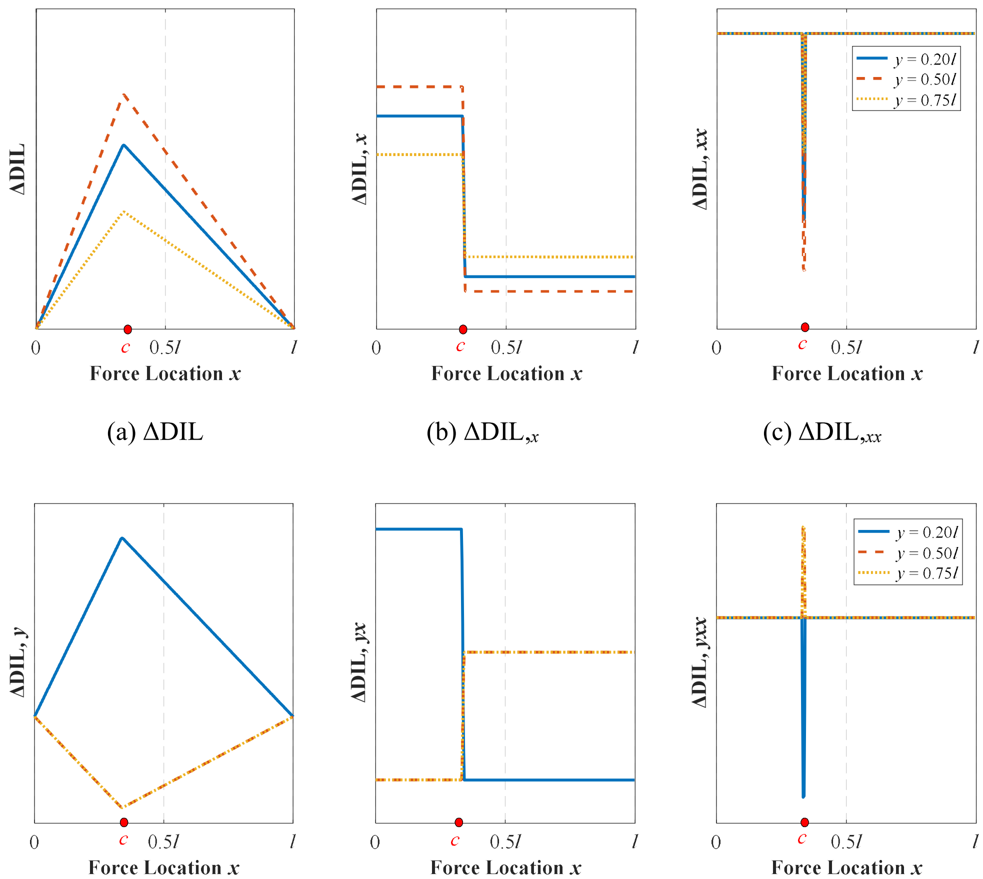

(a) ΔDIL (b) $\Delta\text{DIL}_{,x}$ (c) $\Delta\text{DIL}_{,xx}$

(d) $\Delta\text{DIL}_{,y}$ (e) $\Delta\text{DIL}_{,yx}$ (f) $\Delta\text{DIL}_{,yxx}$

Fig. 5 Representative DIL changes and its first- and second-order derivatives in the simply supported beam.

$\Delta\text{DIL}_{,y}$ (equivalent to ΔRIL) in the undamaged segments are linear functions of x, and the damage location can be identified via the turning point. When the rotation sensor (e.g., tiltmeter) is located on the left or right side of the damage (i.e., $y < (c - \xi)$ or $y > (c + \xi)$), the coefficients of $\Delta\text{DIL}_{,y}$ are always positive or negative, respectively. Thus, the sensitivity of ΔRIL depends on which side the sensor is located in, but is independent of the exact position in each segment (Fig. 5(d)). The damage location in ΔRIL can be further highlighted by calculating the first- or second-order difference of ΔRIL (i.e., $\Delta\text{DIL}_{,yx}$ or $\Delta\text{DIL}_{,yxx}$).

The simply supported beam is a statically determinate structure. Thus, the damage will not cause any changes in bending moment and shear force, as shown by Eqs. (14) and (15), respectively. However, the result will differ if the beam is statically indeterminate, wherein any stiffness change may cause internal load redistribution.

Consequently, $\Delta\text{DIL}_{,yy}$ and $\Delta\text{DIL}_{,yyy}$ (equivalent to ΔBSIL and ΔSSIL) almost exhibit no changes, except in the damaged segment, as shown by Eqs. (16) and (17) and Figs. 4(g) and (j).

When a sensor is installed in the damaged segment (i.e., $(c-\xi) < y < (c+\xi)$), an insightful relationship can be obtained from Eqs. (9) and (14)

$$\alpha = \frac{\Delta EI}{EI} = \frac{\Delta \mathrm{DIL}(x,y)_{,yy}}{\mathrm{DIL}_{\mathrm{d}}(x,y)_{,yy}}, \text{ where } 0<x<l,\ c-\xi \le y \le c+\xi, \tag{18}$$

where the damage coefficient α can be directly estimated by the ratio of the $\Delta\mathrm{DIL}_{,yy}$ to $\mathrm{DIL}_{\mathrm{d},yy}$, thereby indicating the relationship between the damage severity and DIL change ratio.

Eqs. (16) and (17) mean that the damage will not be detected if the strain sensors are not installed at the damage location. Although the recent development of distributed strain sensing using emerging fiber optic sensors may address this need [30,42], it is still regarded as a quite costly solution. It should be emphasized again that the detectable ranges of ΔBSIL and ΔSSIL will vary in a statically indeterminate structure.

However, it does not mean that the conclusion in Eq. (18) is useless. Given the similarity between the $\Delta\mathrm{DIL}_{,xx}$ and $\Delta\mathrm{DIL}_{,yy}$ surfaces in Fig. 4, the $\Delta\mathrm{DIL}_{,xx}$ curve can also be used to quantify the damage coefficient. $\Delta\mathrm{DIL}_{,xx}$ is nonzero when the moving loading passes the damage location $[c-\xi, c+\xi]$,

$$\alpha = \frac{\Delta \mathrm{DIL}(x,y)_{,xx}}{\mathrm{DIL}_{\mathrm{d}}(x,y)_{,xx}}, \text{ where } c-\xi \le x \le c+\xi,\ 0<y<l, \tag{19}$$

which indicates that the damage can be detected even if the sensor location y is different from the damage location. Compared with the extremely narrow detectable range of ΔBSIL indices, $\Delta\mathrm{DIL}_{,xx}$ shows superior performance in the simply supported beam. Moreover, Eq. (19) suggests that the damage coefficient α can be identified on the basis of the DIL measurement alone, where the structural model information is not required.

In general, ΔDIL and ΔRIL exhibit much wider detectable ranges compared with ΔBSIL and ΔSSIL, which agrees with the common view that displacement and strain responses are regarded as global and local damage indices, respectively.

The partial derivatives with respect to x in Fig. 4 correspond to the calculation of finite difference, which may exacerbate the measurement noise effect greatly; whereas the partial derivatives with respect to y correspond to the change of measured quantity by using different types of sensors, which are not associated with the amplification of measurement noise.

In summary, in the considered simply supported beam with single damage, the damage can be identified via the changes in ΔDIL, ΔRIL, and their first- or second-order differences with respect to force location x (i.e., $\Delta\mathrm{DIL}_{,x}$, $\Delta\mathrm{DIL}_{,xx}$, $\Delta\mathrm{RIL}_{,x}$, and $\Delta\mathrm{RIL}_{,xx}$).

More detailed comparisons regarding the sensitivity, detectable range, noise impact, and multi-damage scenarios will be discussed in the succeeding sections by employing a continuous beam example.

3 Damage Sensitivity

Fig. 6 shows a three-span continuous beam that is a typical statically indeterminate structure. The beam with three equal spans *l* and flexural rigidity *EI* is modelled in this section. A unit vertical force is successively applied to the different loading points on the beam along the longitudinal direction. A damaged segment (1.275*l*–1.3*l*) within the central span is simulated, where the sectional height is reduced to represent α = 5% loss in the moment of inertia *I* of the section.

The DIL and RIL functions of the continuous beam are calculated using the static numerical method (global stiffness and moving force matrices). Subsequently, the SIL function is calculated using Eqs. (11) and (12). Based on the calculated IL functions in the intact and damaged states, their sensitivity to damage is discussed systematically, wherein the sensitivity is hereinafter defined as the change in various types of ILs divided by the damage coefficient α and the damage extent ratio β. Greater sensitivities imply that the damage is more likely to be detected [43]. Considering the different magnitudes and units of various types of ILs, these sensitivity results are further normalized by the peak-to-peak amplitude of the corresponding baseline influence surface of each type,

$$s(x,y)=\frac{\Delta \mathrm{IL}(x,y)}{\max\limits_{x,y}\left\{\mathrm{IL}_{\mathrm{u}}(x,y)\right\}-\min\limits_{x,y}\left\{\mathrm{IL}_{\mathrm{u}}(x,y)\right\}}\frac{1}{\alpha\beta}, \tag{20}$$

where ΔIL is the change of different types of ILs; $\max\limits_{x,y}\left\{\mathrm{IL}_{\mathrm{u}}(x,y)\right\}$ and $\min\limits_{x,y}\left\{\mathrm{IL}_{\mathrm{u}}(x,y)\right\}$ are the highest and lowest points of the influence surfaces of different types, respectively, and their difference stands for the peak-to-peak amplitude of the influence surface of the intact beam; α is the damage severity coefficient; and $\beta = 2\xi/3l$ represents the damage extent 2ξ normalized by the total beam length 3*l*. Such normalization enables the dimensionless discussion and comparison of the sensitivity of different types of ILs. The two critical parameters, i.e., damage severity and damage extent, are only used to normalize sensitivity comparison. It needs to be clarified that these IL-based damage indices require only the measured ILs in the intact state and damage state, and the knowledge of damage severity and extend is unnecessary in damage detection.

Damage sensitivities typically change nonlinearly with damage levels (damage severity and extent). Since this observation is well known in the literature, the corresponding discussion is skipped in this study. All the damage sensitivities presented in this section correspond to minor damage levels. Notably, only the findings that are not mentioned in the simply supported beam will be elaborated in this section.

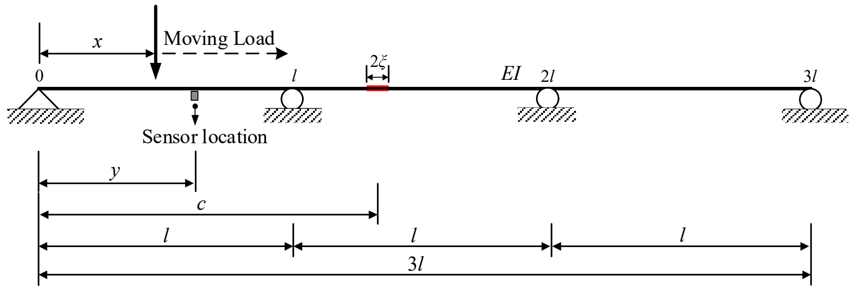

Fig. 6 Schematic of a three-span continuous beam

3.1 DIL and RIL

Figs. 7–8 show the dimensionless sensitivity coefficient surfaces of the ΔDIL and ΔRIL functions, respectively. The two horizontal axes denote the force location x and the sensor location y, respectively. The degree of damage sensitivity is expressed by the colormap.

Similar to the simply supported beam, the property of symmetry about the diagonal line can be observed in the ΔDIL surface in Fig. 7. Given any fixed sensor locations y_i, the peak coefficient of each ΔDIL(x, y_i) curve always occurs at the damage location (i.e., when the force passes the damaged segment), thereby verifying the capability of the ΔDIL index for damage localization. In the central span where the damage occurs, the highest sensitivity occurs when the displacement sensor is installed at the damage location. The peak change in the ΔDIL curve in the central span attenuates with the increasing distance between the sensor and damage locations; and the sensitivity becomes zero at the supports. However, this attenuation trend with the increasing separation distance from the damage cannot be extended to the other spans. In two other side spans, given various sensor locations y_i, the relatively higher and lower sensitivity occur at the mid-span and in the vicinity of support, respectively.

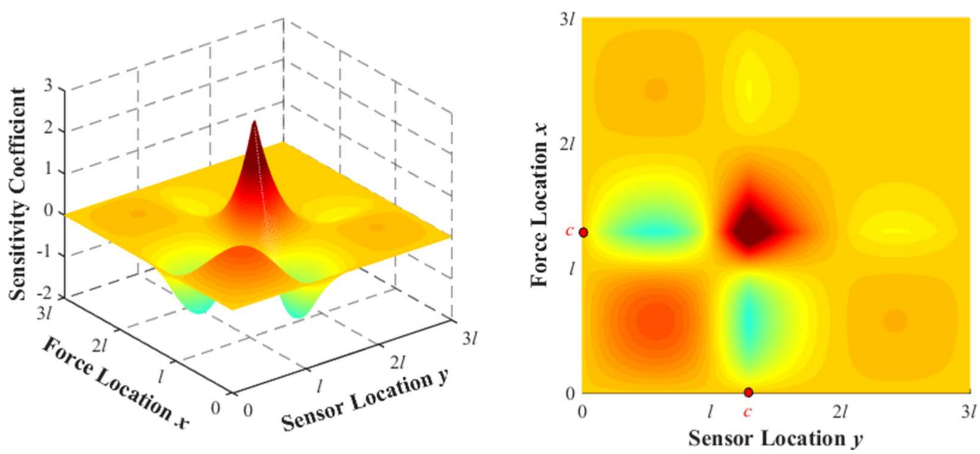

(a) 3D diagram (b) Planar projection

Fig. 7 Dimensionless sensitivity coefficients of ΔDIL in the three-span continuous beam.

Fig. 8 shows the corresponding damage sensitivity of RIL. Some similar observations to that of DIL can be provided. Given any fixed sensor location y_i, a peak that corresponds to the force at the damage location exists in each ΔRIL curve. In the central span with the damage, the sensitivity attenuates with the increasing distance from the damage location; but even at two support locations, the sensitivity is not zero. In two side spans, the sensitivity coefficients are relatively larger near the support rather than at the mid-span.

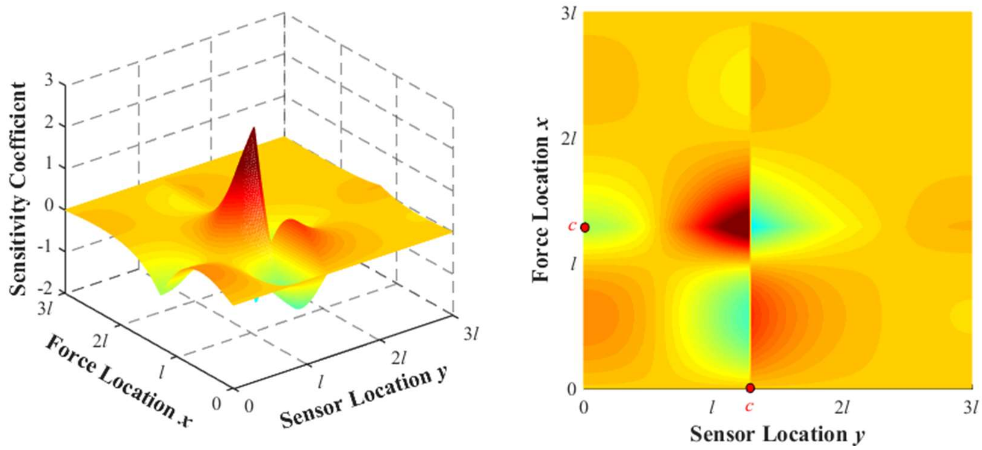

(a) 3D diagram (b) Planar projection

Fig. 8 Dimensionless sensitivity coefficients of ΔRIL in the three-span continuous beam.

3.2 BSIL and SSIL

Figs. 9 and 10 show the dimensionless damage sensitivity of BSIL and SSIL, respectively. When the sensors are installed at the damage locations, the BSIL and SSIL changes will be higher than other sensor locations by at least one order of magnitude. Considering that the installation of the strain sensor at the exact damage location is practically difficult, this scenario is not a typical goal in damage detection studies; and thus the corresponding sensitivity results are excluded in Figs. 9 and 10 so that other parts of the surface can be displayed properly. Unless otherwise stated, such exclusion will be applied to the discussion of any ΔBSIL and ΔSSIL sensitivity in the following sections.

Notably, unlike the conclusion in the simply supported beam, the sensitivity coefficients when the strain sensors are installed at undamaged locations are nonzero because of the redistribution of internal loads in the three-span continuous beam. Therefore, the measurement of bending and shear stress ILs at undamaged locations can also be utilized to detect damage in statically indeterminate beams.

Fig. 9 shows that when the sensor location is near the second support (i.e., $y = l$) that is closer to the damage, the ΔBSIL curve exhibits the highest damage sensitivity. The sensitivity coefficients generally attenuate with the increasing distance between the second support and the sensor locations. Nevertheless, the ΔBSIL is less sensitive to the damage than ΔDIL and ΔRIL in terms of the peak values of the sensitivity coefficients shown in Figs. 7 and 8.

Fig. 10 shows that the ΔSSIL curves vary when sensors are installed in different spans but are identical when sensors are installed in the same span. Such observation indicates that ΔSSIL is not sensitive to the sensor locations. However, the overall magnitude of the ΔSSIL sensitivity coefficient is lower than those of the other types of ILs.

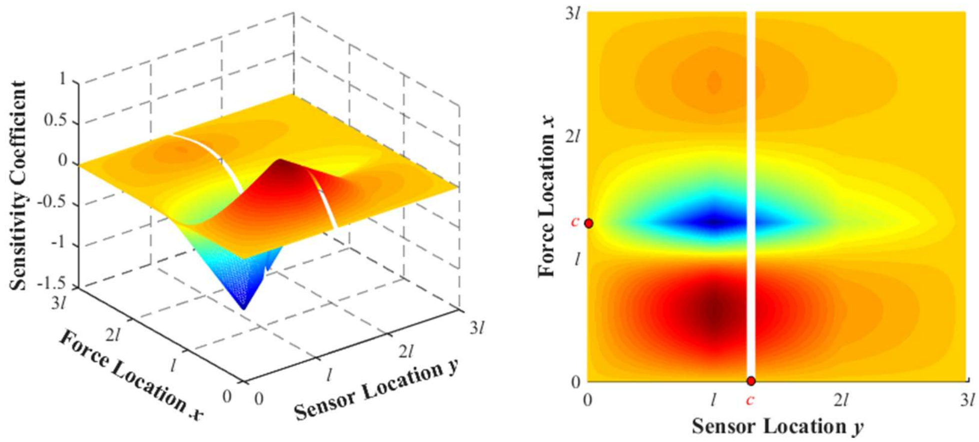

(a) Excluding sensor in damage location (b) Planar projection

Fig. 9 Dimensionless sensitivity coefficients of ΔBSIL in the three-span continuous beam (the sensors installed at the damage location are excluded).

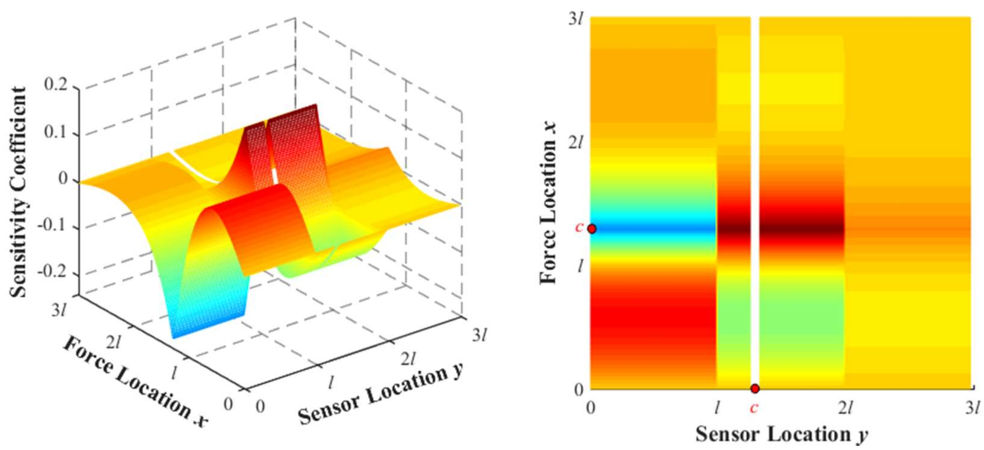

(a) Excluding sensor in damage location (b) Planar projection

Fig. 10 Dimensionless sensitivity coefficients of ΔSSIL in the three-span continuous beam (the sensors installed at the damage location are excluded).

3.3 Finite Difference of IL

3.3.1 Single-damage Scenario

In addition to various types of ILs, the finite differences of ILs have also been explored as damage indices. Fig. 11 illustrates the dimensionless sensitivity curves for the finite difference results of ΔDIL, wherein the three sensor locations are selected as the relatively sensitive locations for DIL.

Given a displacement sensor location y_i, the ΔDIL curve in Fig. 7 exhibits multiple peaks, only one of which corresponds to the damage locations. In Fig. 11, the finite differences of ΔDIL can not only improve the damage sensitivity in comparison to ΔDIL but also highlight the damage locations more clearly by exhibiting much more significant fluctuations when the force location x approaches the damage location. The coefficient curves of $\Delta\text{DIL}_{,x}$ exhibit a sudden change (drop or rise) at the damage location, whereas $\Delta\text{DIL}_{,xx}$ exhibits a unique peak in the damage segment $[c-\xi, c+\xi]$. The coefficient of the selected $\Delta\text{DIL}_{,xx}$ reaches up to 20 when the moving force acts on the damage location, although it attenuates rapidly when the force gets away from the damage location. Thus, damage localization can be realized via these characteristics in the coefficient magnitude. Similar to the simply supported beam, the sensitivity curves of $\Delta\text{DIL}_{,x}$ and ΔRIL (i.e., $\Delta\text{DIL}_{,y}$) are similar in terms of magnitude and trend but in different observation directions.

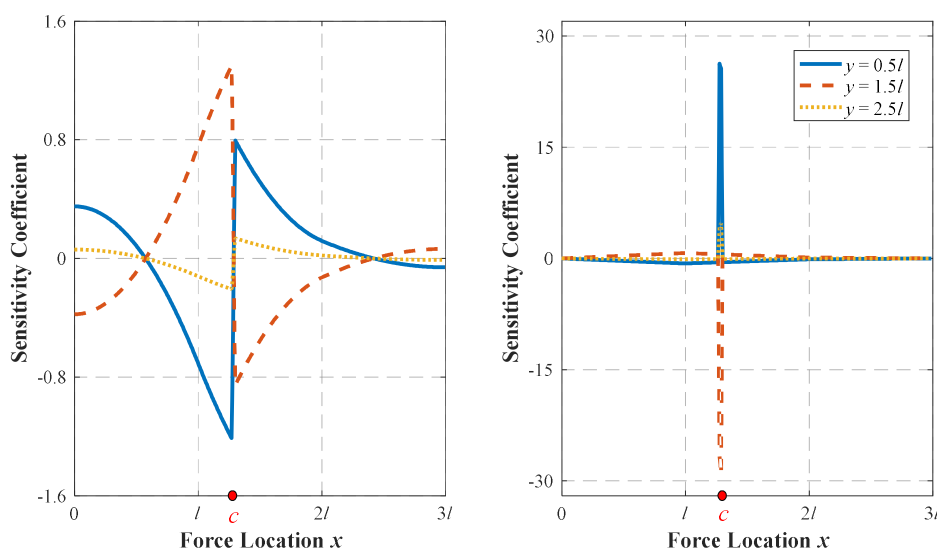

(a) First-order $\Delta\text{DIL}_{,x}$ (b) Second-order $\Delta\text{DIL}_{,xx}$

Fig. 11 Representative dimensionless sensitivity coefficients of finite difference of ΔDIL in the three-span continuous beam.

Some similar observations can be made to the finite differences of other types of ΔIL.

Given a sensor location y_i, the finite differences of ΔRIL, ΔBSIL, and ΔSSIL can locate damage via the sudden change in the coefficient magnitude. Moreover, the calculation of the finite differences can enhance the sensitivity of ΔRIL; however, the finite differences of ΔBSIL and ΔSSIL results in low sensitivity results. The corresponding figures are not presented in this study because of page limits.

3.3.2 Multi-damage Scenario with Measurement Noise

In addition to the original damaged segment, another new damaged segment (0.6–0.625l) is introduced with a flexural rigidity reduction of 5% to simulate a multi-damage scenario. Given that the shapes of ΔIL and their finite difference at a given sensor location are similar, only the analysis results of ΔDIL are elaborated as an example. In particular, the noise-contaminated ΔDIL^* was considered

$$\Delta\text{DIL}^* = \Delta\text{DIL} + \eta\gamma N_{\text{noise}}, \tag{21}$$

where η is the noise level, γ is the average of the ΔDIL, and N_{noise} refers to a random variable that follows a Gaussian distribution between [−1, 1]. The measurement noise level of η = 7.5%, which is consistent with the experimental results previously reported by the authors [28], is introduced in this study. Notably, the static measurement noise level is typically low, considering the common dynamic measurement noise can be effectively removed or minimized by averaging signals in a sufficient period.

Fig. 12 shows the DIL-based indices with and without noise interference when the deflection sensor is installed at y = 1.5l. Three peaks appear in the coefficient curve of ΔDIL, out of which, two sharp peaks correspond to the simulated double damages (Fig. 12(a)). The calculations of $\Delta\text{DIL}_{,x}$ or $\Delta\text{DIL}_{,xx}$ highlight two sudden changes in the curve that correspond to damage locations accurately.

However, the superiority of the finite difference indices in terms of sensitivity and localization should be interpreted more carefully. In Fig. 12, the finite difference computation amplifies the noise effect. $\Delta\text{DIL}_{,x}$ can still identify the sharp changes near the damage locations fairly well, indicating that $\Delta\text{DIL}_{,x}$ will be a promising damage indicator in multi-damage scenarios; whereas $\Delta\text{DIL}_{,xx}$ cannot capture the damage location information anymore because of the noise effect. Similar observations can be made for other types of ILs.

The noise amplification may limit the application of finite difference-based indices at a high noise level. Denoising methods, such as iterative multi-parameter Tikhonov regularization [44] and Sparse regularization [45], may be applied to reduce the noise effect before or after the computation of high-order finite difference and achieve satisfactory anti-noise robustness. In the numerical or experimental studies in this paper, a simple smoothing method by using a larger interval "$n\Delta x$" ($n \geq 1$) is applied to mitigate the noise effect, which is equivalent to an averaging process.

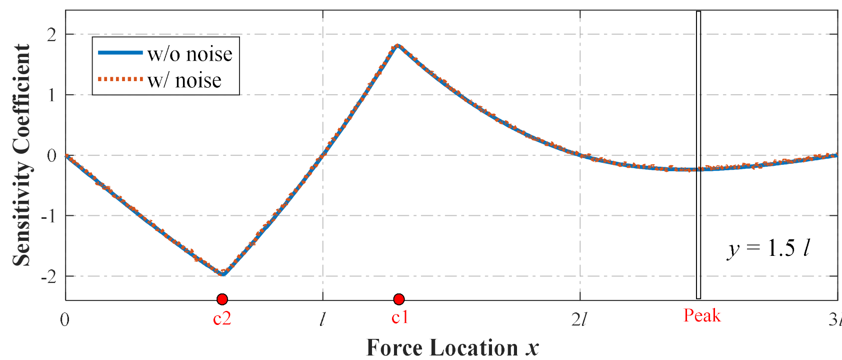

(a) ΔDIL

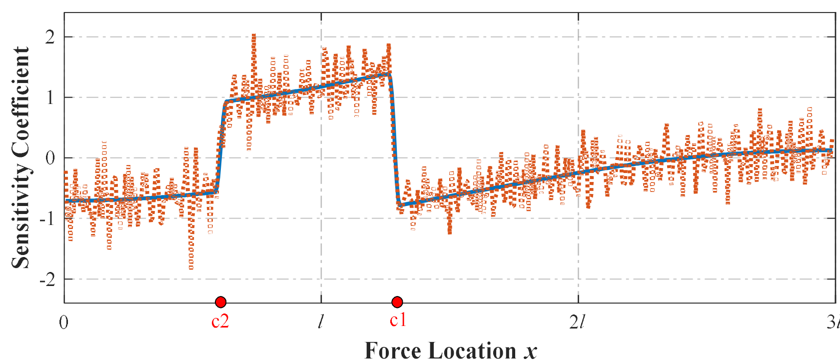

(b) $\Delta\text{DIL}_{,x}$

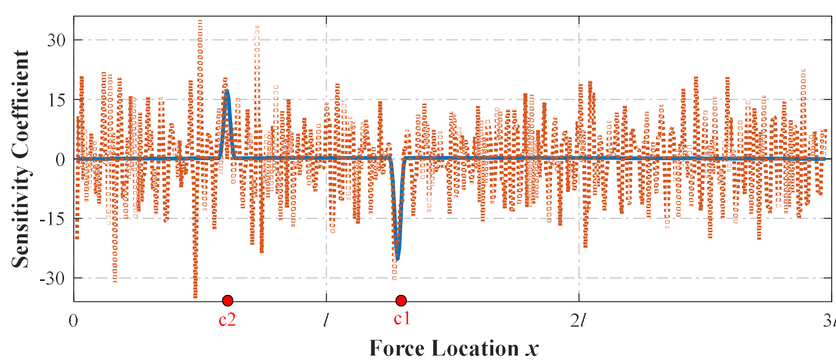

(c) $\Delta\text{DIL}_{,xx}$

Fig. 12 Detection performance of DIL-based indices in the three-span continuous beam.

4 Detectable Range for Variable Damage Locations

The discussions in Sections 2 and 3 are based on fixed damage locations (single or double). Considering practically unknown damage locations in a beam, this section examines the damage sensitivity with varying damage locations. Subsequently, the effective detectable ranges are evaluated considering the different types of ILs, sensor locations, and damage locations, wherein detectable range refers to the range of detectable damage locations with one specific sensor location.

The detectable range is judged by the magnitude of the dimensionless sensitivity coefficient s in Eq. (20). Our previous experimental study [28] reported that a single damage in a simply supported beam could be detected accurately by using the ΔDILs measured at 1/4, 1/2, and 3/4 spans. The corresponding peak sensitivity coefficients s are estimated as 1.5, 2.5, and 5.2 for the three sensor locations. A conservative threshold of 1.5 is suggested to determine the detectable range, indicating that the required change ratio of $\Delta \mathrm{IL}(x,y) \Big/ \left\{ \max\limits_{x,y}\{\mathrm{IL_u}(x,y)\} - \min\limits_{x,y}\{\mathrm{IL_u}(x,y)\} \right\}$ is approximately 0.125% for successful damage detection, given the damage severity of $\alpha = 10\%$ and damage extent ratio of $\beta = 1/120$. Notably, this threshold is essentially related to the precision of the used sensors.

Table 1 Detectable damage range with different sensor locations

Types of ILs	Sensor Location (×l)	Detectable Range (×l)	Ratio* (%)
DIL	0.25	0.125–0.65	17.5
	0.5	0.175–0.75, 0.975–1.45	35.0
	0.75	0.275–0.825; 1–1.4	31.7
	1.25	0.575–0.775; 1.175–1.625	21.7
	1.5	0.55–0.8; 1.25–1.75; 2.2–2.45	33.3
RIL	0 (support)	0.05–0.625	19.2
	0.25	0.225–0.65	14.2
	0.5	0.25–0.7	15.0
	0.75	0.275–0.825	18.3
	1 (support)	0.425–0.925; 0.975–1.475	33.3
	1.25	1.15–1.625	15.8
	1.5	1.275–1.725	15.0
BSIL	0.75	0.5–0.85, 1–1.025; 1.075–1.35;	21.7
	1 (support)	0.4–1.45	35.0
	1.25	0.6–0.75, 1.125–1.425	15.0
SSIL	all	Sensor Location	< 0.1

*Ratio is the percentage of this detectable range to the total length 3l of the beam.

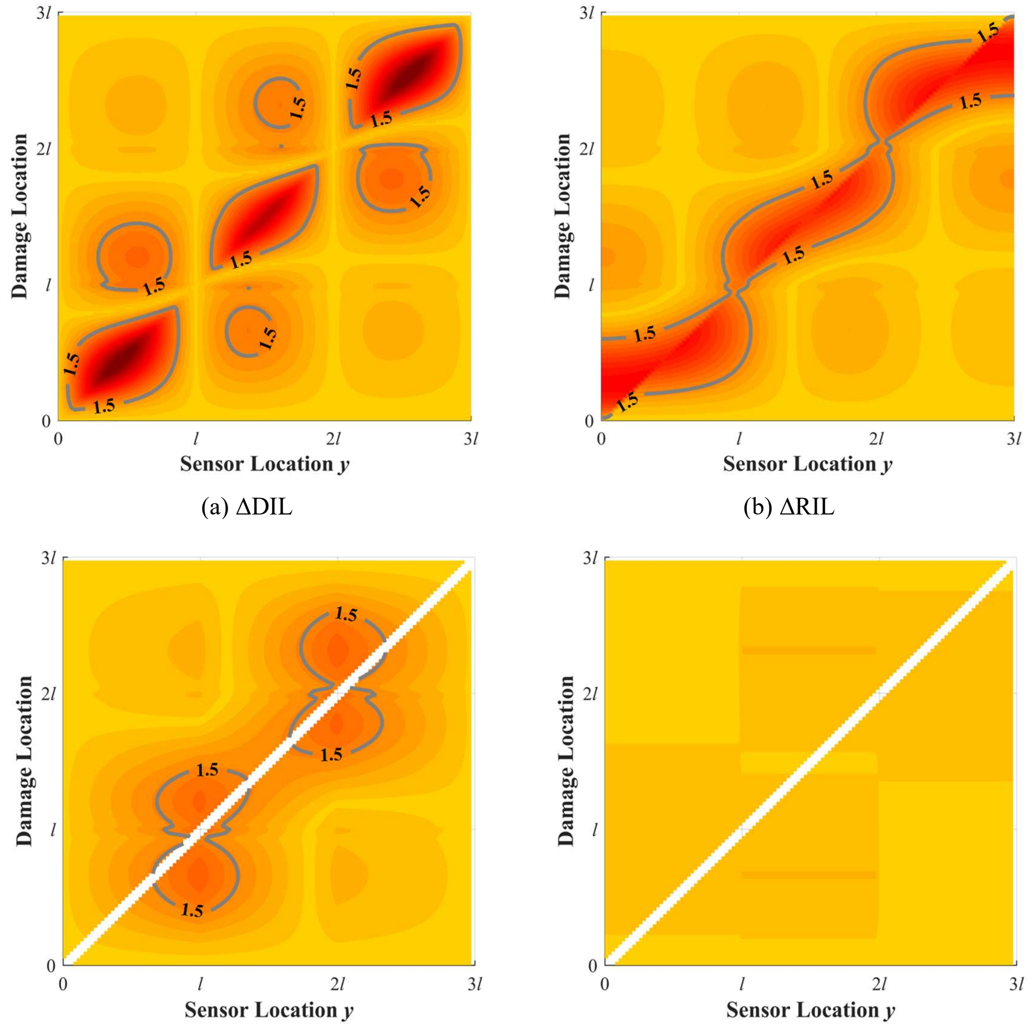

(a) ΔDIL (b) ΔRIL

(c) ΔBSIL (d) ΔSSIL

Fig. 13 Detectable damage range of different types of ILs shown in the $s_{\text{p-p}}$ plot for the three-span continuous beam.

Given an assumed damage location c_i and a sensor location y_i, the sensitivity curve $s(x, y_i)$ for each IL can be computed as a function of x according to Eq. (20). Then, the peak-to-peak amplitude of the curve will be computed as $s_{\text{p-p}} = \max_x \{s(x, y_i)\} - \min_x \{s(x, y_i)\}$. If $s_{\text{p-p}} \geq 1.5$, then the damage location c_i is regarded to be detectable at the sensor location y_i. By varying the damage and sensor locations, the distributions of $s_{\text{p-p}}$ for different types of ILs can be obtained (Fig. 13). Consequently, the detectable range that corresponds to the assumed threshold can be determined.

The diagonal values in the four graphs in Fig. 13 are always the largest, indicating that the ILs measured at damage locations are the most sensitive to the damage. The contour line of $s_{\text{p-p}} = 1.5$ in Fig. 13 clearly indicates the detectable range of different sensor locations. Table 1 summarizes the detectable ranges at several key sensor locations. Considering the symmetry of the three-span continuous beam, only sensor locations in the left half of the beam are presented.

The detectable ranges of ΔDIL are largest when the displacement sensor is installed in the middle of the first and second span; whereas the largest detectable range of ΔRIL is achieved when the rational sensor is deployed at the support. The highest ratios of the detectable ranges using ΔDIL and ΔRIL are similar (≈ 30%), despite the different distributions of their detectable range.

ΔBSIL near the middle support (0.75–1.25*l*) has relatively larger detectable ratio, whereas that measured at other sensor locations can only reflect damage that exactly occurs at the sensor location. Thus, the sensor locations of ΔBSIL that can locate damage are considerably narrower in comparison with those of ΔDIL and ΔRIL. ΔSSIL may not be suitable for damage detection because of its extremely narrow detectable range.

Notably, ΔDIL can hardly detect damages close to the supports; while ΔRIL and ΔBSIL can if the sensors are deployed at proper locations. The complementary characteristics of ΔDIL, ΔRIL, and ΔBSIL suggest that the deployment of multiple types of sensors can enlarge the detectable range and improve damage detection results.

5 Simply Supported Beam Experiment

A simply supported stainless steel beam was tested in this section to validate the effectiveness of the various types of IL-based indices. The beam had a total length of 650 mm (a major span of 600 mm between two supports) and a cross-section of 25 mm × 3 mm. The beam was equally divided into 65 segments, with each segment 10 mm long. In addition to the intact beam, a damage scenario was also tested, in which the width of the cross section was reduced in the 19th segment.

Fig. 14(a) shows the layout of the experimental setup, and Fig. 14(b) shows the corresponding experimental photographs. The laser displacement sensors (model No. KEYENCE LK-500) were installed at the 18th, 25th, 33rd, and 48th nodes, which corresponded to the 1/4, 1/2, and 3/4 positions of the main span. Four strain gauges were placed at the same locations as the laser displacement sensors, but with an additional one at the 9th node. The dial gauges (model No. Mitutoyo 543-790) were placed at the 5th and 65th nodes to measure the displacement and then compute the rotation angle of the supports. A KYOWA data acquisition system (model No. EDX-100) was used to collect the displacement and strain signals at a sampling rate of 10 Hz. Due to the page limit, only part of the experimental results is presented in this paper.

Fig. 15 shows the measured DILs, RILs, and strain ILs at different locations in an intact state. Taking the DIL at the 25th node as an example, Fig. 16 shows the DIL change and its first-order finite difference when the single damage was introduced. As aforementioned, a simple smoothing method was applied to mitigate the noise amplification effect.

Even with the presence of the measurement noise, the ΔDIL and its first-order finite difference can still satisfactorily locate the damage, which demonstrates the feasibility of using these IL-based indices for damage localization. Note that the measured DIL results at the 18th, 33rd, and 48th nodes can successfully locate damage as well. However, the noise effect in the second-order finite difference was too significant, which prevented successful damage detection in the experimental case.

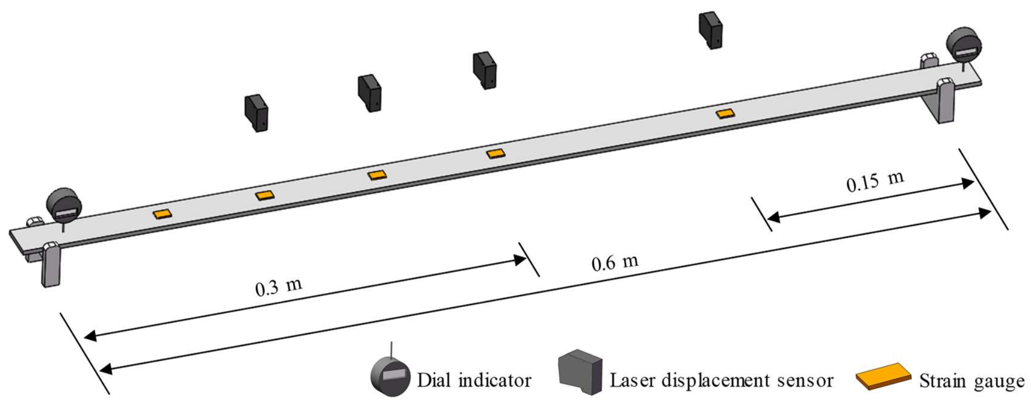

(a) Layout of experimental setup.

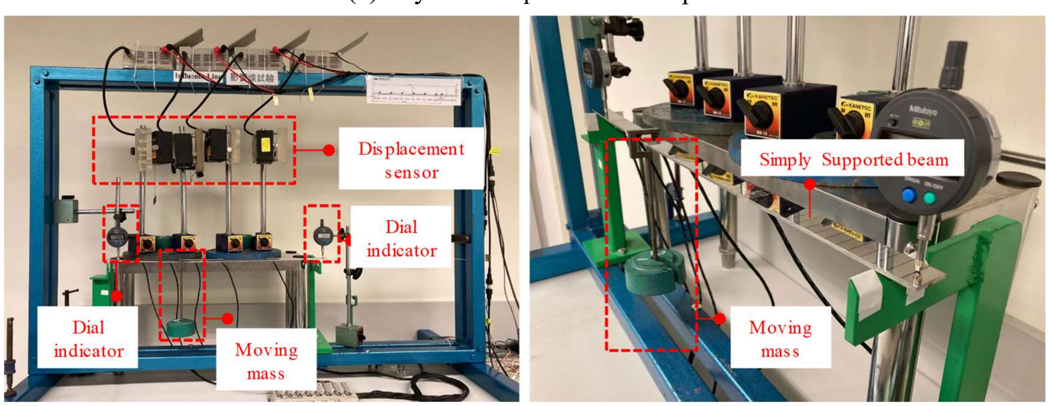

(b) Photograph of experimental setup

Fig. 14 Experimental setup of a simply supported beam.

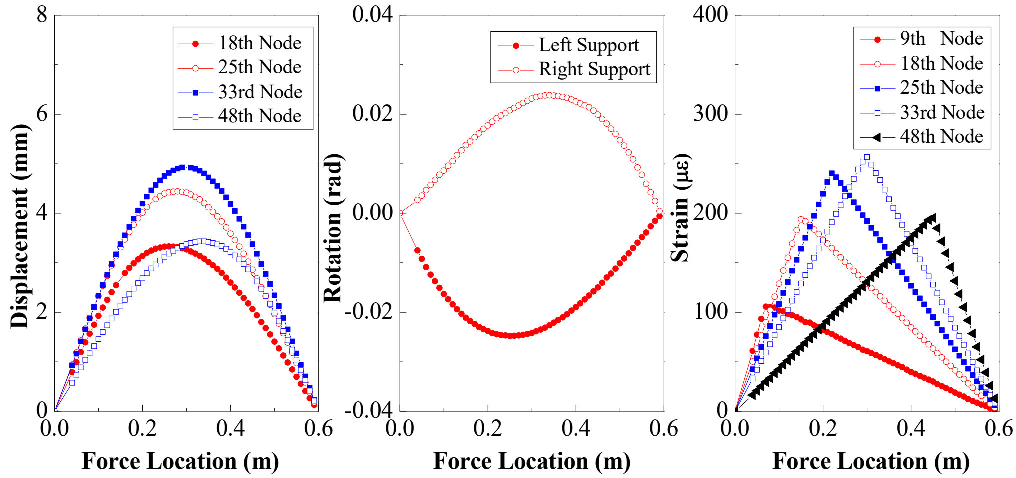

(a) DILs (b) RILs (c) Strain ILs

Fig. 15 IL measurement in an intact state of the tested beam.

Similarly, Fig. 17 shows the damage detection result using the ΔRIL-based indices measured at the left support, which is closer to the damage than the right one. Both ΔRIL and its first-order finite difference can locate damage fairly well. Fig. 18 shows the detection results using the strain ILs. Only the strain IL measured in the damaged segment can identify damage, which confirms the finding that strain IL is not suitable for damage detection in a simply supported beam (or any statically determinate beam).

These experimental results partially validate the feasibility and effectiveness of using IL changes (including ΔDIL and ΔRIL) and their corresponding first-order finite difference in damage identification in a simply supported beam.

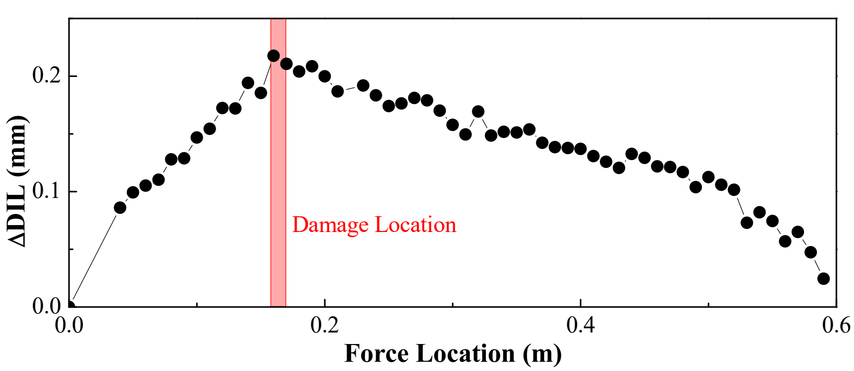

(a) ΔDIL

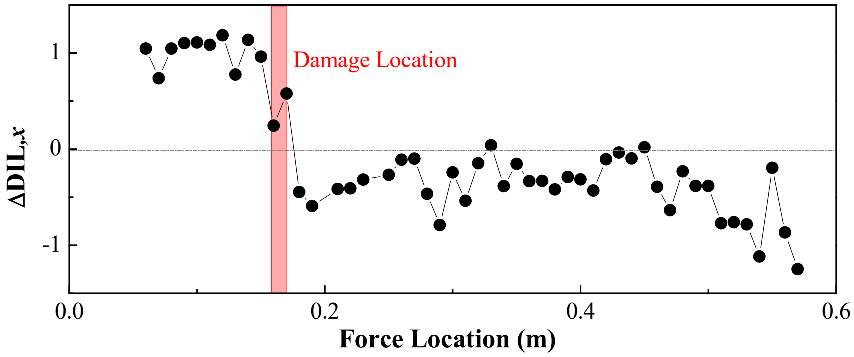

(b) $\Delta\mathrm{DIL}_{,x}$

Fig. 16 The damage-induced changes of DIL-based indices measured at the 25th node of the tested beam.

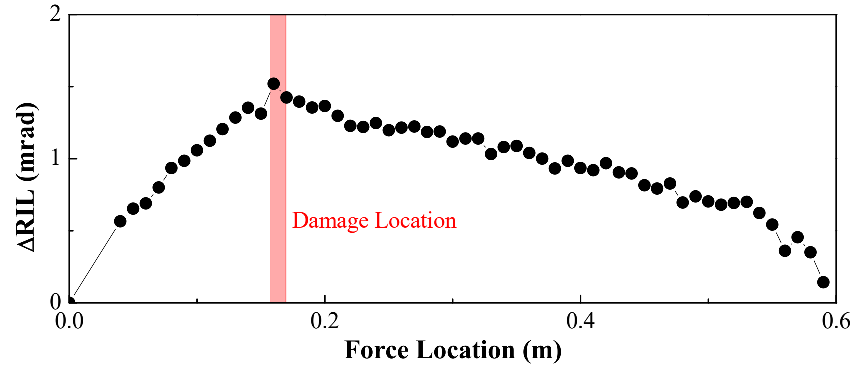

(a) ΔRIL

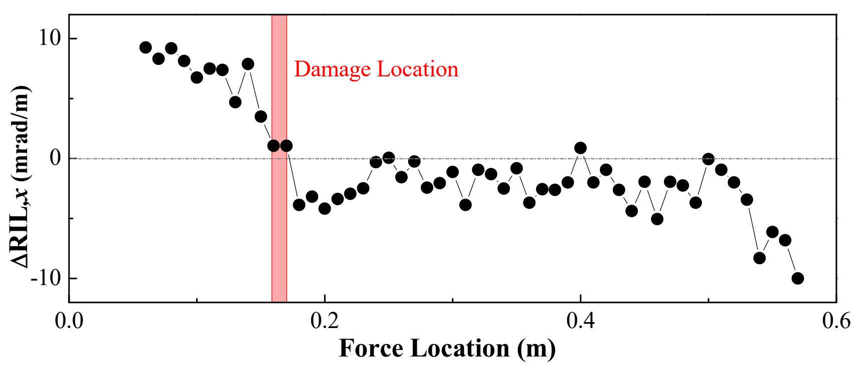

(b) $\Delta\mathrm{RIL}_{,x}$

Fig. 17 The damage-induced changes of RIL-based indices measured at the left support of the tested beam.

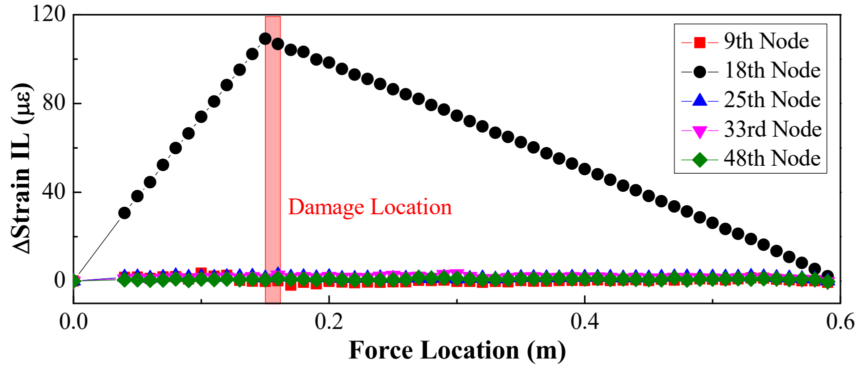

Fig. 18 The damage-induced changes of strain IL-based indices in the tested beam.

6 Conclusions

This paper investigates a series of IL-based damage indices, including DIL, RIL, BSIL, SSIL, and their corresponding first- and second-order finite differences. The intrinsic relationships among different types of ILs are revealed for the first time to illustrate their similarities and differences. The normalized sensitivities and detectable ranges of different types of ILs are evaluated through numerical examples of a simply supported beam and a three-span continuous beam. An experiment on a simply supported beam was performed to validate the effectiveness of different types of IL-based damage indices. The major results and findings are summarized as follows:

For the simply supported beam case:

(1) RIL and DIL can be used to detect damage; whereas BSIL and SSIL cannot detect damage unless the damage occurs at the sensor location. In this regard, RIL and DIL are superior in terms of their relatively wide detectable range.

(2) The finite differences (first- or second-order) of ΔDIL with respect to the force location can highlight the damage locations by showing the dramatic changes in the magnitude of the curves.

(3) Other types of ILs (i.e., ΔRIL, ΔBSIL, and ΔSSIL) can be expressed as partial derivatives of ΔDIL of different orders with respect to y-direction (sensor location); meanwhile, the finite differences can be expressed as partial derivatives with respect to x-direction (force location). This finding reveals the intrinsic relationships between ΔRIL and the first-order difference of ΔDIL and between ΔBSIL and the second-order difference of ΔDIL. These results essentially represent the observations of the same surface in different directions, thereby showing the similarities and differences in the results.

(4) Damage coefficient is theoretically equal to the ratio of $\Delta DIL_{,xx}$ (i.e., the second-order difference of DIL change) to the $DIL_{,xx}$ in the damage state, which provides a useful model-

free method for damage detection in the simply supported beam.

(5) The IL changes (including ΔDIL and ΔRIL) and their first-order finite difference can successfully locate damage in the experimental case.

For the continuous beam that represents a statically indeterminate bridge:

(1) If the sensor and damage are in the same span, then the damage sensitivity of DIL and RIL is mainly influenced by the distance between the sensor and damage locations; if the sensor is installed in other spans, the DIL measured at the mid-span and RIL at the support exhibit relatively great sensitivity.

(2) Considering the redistribution of internal loads, BSIL and SSIL, even when installed at undamaged locations, exhibit the changes induced by damage. BSIL measured at the nearest support to the damage has the highest sensitivity. The sensitivity of SSIL depends on which span the sensor is located in but is independent of the exact position in each span.

(3) Calculating the finite differences of ΔDIL and ΔRIL can enhance damage sensitivity and highlight damage locations through the sudden changes in the curves. However, such calculations may also amplify the noise interference. The first-order difference is suggested in damage detection in consideration of a balance between the sensitivity and noise interference. Noise filtering operation should be performed when high-order difference is desirable.

(4) Considering variable damage locations, ΔDIL measured at the middle of each span shows a relatively wide detectable range; whereas ΔRIL and ΔBSIL measured near the middle support have larger detectable ranges; ΔSSIL can detect damage that only appears at the sensor location. These observations suggest different optimal installation locations for displacement transducers, tiltmeters, and strain gauges in the beam. The complementary characteristics of various types of ILs also suggest the benefits of deploying multiple types of sensors for the detection of beam damages.

It needs to be pointed out that this study focused on the analytical revelation based on simple beam models and ideal data setting. Although a simple test partially verified the findings in the simply supported beam, systematic experimental studies need to be conducted in the future to compare different types of ILs in damage detection for more complex structures in the laboratory and in-situ environments.

Acknowledgment

The authors are grateful for the financial supports provided by the National Key R&D Program of China (2019YFB1600700), the National Natural Science Foundation of China

(NSFC-51778550), GDSTC Key Technologies R&D Program (2019B111106001), and the Research Grants Council of Hong Kong (T22-502/18-R). The first author also gratefully acknowledges the support from the Postdoc Matching Fund Scheme from the Hong Kong Polytechnic University (W21P-P0039437). The findings and opinions expressed in this paper are from the authors alone and are not necessarily the views of the sponsors.

Data Availability

All data, models, and code generated or used during the study appear in the submitted article.

References

[1] Gómez-Martínez R, Sánchez-García R, Escobar-Sánchez, JA, Arenas-García LM, Mendoza-Salas MA, Rosales-González ON. Monitoring two cable-stayed bridges during load tests with fiber optics. Structures 2021; 33: 4344-4358. https://doi.org/10.1016/j.istruc.2021.07.026.

[2] Zhang YM, Wang H, Bai Y, Mao JX, Xu YC. Bayesian dynamic regression for reconstructing missing data in structural health monitoring. Struct Health Monit, 2022; 14759217211053779. https://doi.org/10.1177/14759217211053779

[3] Bernal D. Damage localization and quantification from the image of changes in flexibility. J Eng Mech 2014; 140(2): 279-286. https://doi.org/10.1061/(ASCE)EM.1943-7889.0000617.

[4] Doebling SW, Farrar CR, Prime MB. A summary review of vibration-based damage identification methods. Shock Vib Dig 1998; 30(2): 91-105. https://doi.org/10.1177/058310249803000201.

[5] Zou Y, Tong L, Steven GP. Vibration-based model-dependent damage (delamination) identification and health monitoring for composite structures—a review. J Sound Vib 2000; 230(2): 357-378. https://doi.org/10.1006/jsvi.1999.2624.

[6] Cao L, He WY, Ren WX. Damage localization and quantification for beam bridges based on frequency variation of parked vehicle-bridge systems. Structures 2021; 31: 357-368. https://doi.org/10.1016/j.istruc.2021.01.098.

[7] Cawley P, Adams RD. The location of defects in structures from measurements of natural frequencies. J Strain Anal Eng Des 1979; 14(2): 49-57. https://doi.org/10.1243/03093247V142049.

[8] Gorgin R. Damage identification technique based on mode shape analysis of beam structures. Structures 2020; 27: 2300-2308. https://doi.org/10.1016/j.istruc.2020.08.034.

[9] Liu X, Lieven N, Escamilla-Ambrosio PJ. Frequency response function shape-based methods for structural damage localisation. Mech Syst Signal Pr 2009; 23(4): 1243-1259. https://doi.org/10.1016/j.ymssp.2008.10.002.

[10] Chinka SSB, Putti SR, Adavi BK. Modal testing and evaluation of cracks on cantilever beam using mode shape curvatures and natural frequencies. Structures 2021; 32: 1386-1397. https://doi.org/10.1016/j.istruc.2021.03.049.

[11] Shi Z, Law S, Zhang L. Structural damage localization from modal strain energy change. J Sound Vib 1998; 218(5): 825-844. https://doi.org/10.1006/jsvi.1998.1878.

[12] Chen ZW, Zhu S, Xu YL, Li Q, Cai QL. Damage detection in long suspension bridges using stress influence lines. J Bridge Eng 2015; 20(3): 05014013. https://doi.org/10.1061/(ASCE)BE.1943-5592.0000681.

[13] Majumder L, Manohar C. Nonlinear reduced models for beam damage detection using data on moving oscillator–beam interactions. Comput Struct 2004; 82(2-3): 301-314. https://doi.org/10.1016/j.compstruc.2003.08.007.

[14] Ouyang H. Moving-load dynamic problems: A tutorial (with a brief overview). Mech Syst Signal Pr 2011; 25(6): 2039-2060. https://doi.org/10.1016/j.ymssp.2010.12.010.

[15] He WY, Ren WX, Zhu S. Damage detection of beam structures using quasi-static moving load induced displacement response. Eng Struct 2017; 145: 70-82. https://doi.org/10.1016/j.engstruct.2017.05.009.

[16] He WY, Zhu S, Ren WX. Two-phase damage detection of beam structures under moving load using multi-scale wavelet signal processing and wavelet finite element model. Appl Math Model 2019; 66: 728-744. https://doi.org/10.1016/j.apm.2018.10.005.

[17] Link M, Weiland M. Damage identification by multi-model updating in the modal and in the time domain. Mech Syst Signal Pr 2009; 23(6): 1734-1746. https://doi.org/10.1016/j.ymssp.2008.11.009.

[18] Li J, Zhao X. A super-element approach for structural identification in time domain. Front Mech Eng China 2006; 1(2): 215-221. https://doi.org/10.1007/s11465-006-0004-4.

[19] Catbas FN, Aktan, AE. Condition and damage assessment: issues and some promising indices. J Struct Eng 2002; 128(8): 1026-1036. https://doi.org/10.1061/(ASCE)07339445(2002)128:8(1026).

[20] AASHTO. The manual for bridge evaluation, (2nd Edition), American Association of State Highway and Transportation Officials Subcommittee on Bridges Structures, Washington DC, USA; 2011. https://civilnode.com/download-book/10247753866294/manual-for-bridge-evaluation-2nd-edition

[21] Lansdell A, Song W, Dixon B. Development and testing of a bridge weigh-in-motion method considering nonconstant vehicle speed. Eng Struct 2017; 152, 709-726. https://doi.org/10.1016/j.engstruct.2017.09.044.

[22] Strauss A, Wendner R, Frangopol DM, Bergmeister K. Influence line-model correction approach for the assessment of engineering structures using novel monitoring techniques. Smart Struct Syst 2012; 9(1): 1-20. https://doi.org/10.12989/sss.2012.9.1.001.

[23] Zhu Q, Xu Y, Xiao X. Multiscale modeling and model updating of a cable-stayed bridge. I: Modeling and influence line analysis. J Bridge Eng 2015; 20(10): 04014112.

https://doi.org/10.1061/(asce)be.1943-5592.0000722.

[24] Zaurin R, Catbas FN. Integration of computer imaging and sensor data for structural health monitoring of bridges. Smart Mater Struct 2009; 19(1): 015019. https://doi.org/10.1088/0964-1726/19/1/015019.

[25] Zaurin R, Catbas FN. Structural health monitoring using video stream, influence lines, and statistical analysis. Struct Health Monit 2011; 10(3): 309-332. https://doi.org/10.1177/1475921710373290.

[26] Zaurin R, Khuc T, Catbas FN. Hybrid sensor-camera monitoring for damage detection: case study of a real bridge. J Bridge Eng 2016; 21(6): 05016002. https://doi.org/10.1061/(asce)be.1943-5592.0000811.

[27] Zhu S, Chen ZW, Cai Q, Lei Y, Chen B. Locate damage in long-span bridges based on stress influence lines and information fusion technique. Adv Struct Eng 2014; 17(8): 1089-1102. https://doi.org/10.1260/1369-4332.17.8.1089.

[28] Chen ZW, Cai Q, Zhu S. Damage quantification of beam structures using deflection influence lines. Struct Contr Health Monit 2018; 25(11): e2242. https://doi.org/10.1002/stc.2242.

[29] Zeinali Y, Story BA. Framework for flexural rigidity estimation in Euler-Bernoulli beams using deformation influence lines. Infrastructures 2017; 2(4): 23. https://doi.org/10.3390/infrastructures2040023.

[30] Alamdari MM, Kildashti K, Samali B, Goudarzi HV. Damage diagnosis in bridge structures using rotation influence line: Validation on a cable-stayed bridge. Eng Struct 2019a; 185: 1-14. https://doi.org/10.1016/j.engstruct.2019.01.124.

[31] Huseynov F, Kim C, OBrien E, Brownjohn J, Hester D, Chang K. Bridge damage detection using rotation measurements–Experimental validation. Mech Syst Signal Pr 2020; 135: 106380. https://doi.org/10.1016/j.ymssp.2019.106380.

[32] Chen ZW, Yang W, Li J, Cheng Q, Cai Q. A systematic method from influence line identification to damage detection: Application to RC bridges. Comput Concr 2017; 20(5): 563-572. https://doi.org/10.12989/cac.2017.20.5.563.

[33] Zhou Y, Di S, Xiang C, Li W, Wang L. Damage identification in simply supported bridge based on rotational-angle influence lines method. Trans Tianjin Univ 2018; 24(6): 587-601. https://doi.org/10.1007/s12209-018-0135-9.

[34] Alamdari MM, Ge L, Kildashti K, Zhou Y, Harvey B, Du Z. Non-contact structural health monitoring of a cable-stayed bridge: case study. Struct Infrastruct Eng 2019b; 15(8): 1119-1136. https://doi.org/10.1080/15732479.2019.1609529.

[35] Wang NB, Ren WX, Huang TL. Baseline-free damage detection method for beam structures based on an actual influence line. Smart Struct Syst 2019; 24(4): 475-490. https://doi.org/10.1016/j.jsv.2014.04.056.

[36] Chen ZW, Cai QL, Li J. Stress influence line identification of long suspension bridges installed with structural health monitoring systems. Int J Struct Stab Dyn 2016; 16(04):

1640023. https://doi.org/10.1142/S021945541640023X.

[37] Wang NB, He LX, Ren WX, Huang TL. Extraction of influence line through a fitting method from bridge dynamic response induced by a passing vehicle. Eng Struct 2017; 151: 648-664. https://doi.org/10.1016/j.engstruct.2017.06.067.

[38] Frøseth GT, Rønnquist A, Cantero D, Øiseth O. Influence line extraction by deconvolution in the frequency domain. Comput Struct 2017; 189: 21-30. https://doi.org/10.1016/j.compstruc.2017.04.014.

[39] Zheng X, Yang DH, Yi TH, Li HN. Bridge influence line identification from structural dynamic responses induced by a high−speed vehicle. Struct Contr Health Monit 2020; e2544. https://doi.org/10.1002/stc.2544.

[40] Zheng X, Yang DH, Yi TH, Li HN. Development of bridge influence line identification methods based on direct measurement data: A comprehensive review and comparison. Eng Struct 2019; 198: 109539. https://doi.org/10.1016/j.engstruct.2019.109539.

[41] Hu N, Dai GL, Yan B, Liu K. Recent development of design and construction of medium and long span high-speed railway bridges in China. Eng Struct 2014; 74: 233-241. https://doi.org/10.1016/j.engstruct.2014.05.052.

[42] Wu B, Wu G, Lu H, Feng DC. Stiffness monitoring and damage assessment of bridges under moving vehicular loads using spatially-distributed optical fiber sensors. Smart Mater Struct 2017; 26(3): 035058. https://doi.org/10.1088/1361-665x/aa5c6f.

[43] Zhao J, DeWolf JT. Sensitivity study for vibrational parameters used in damage detection. J Struct Eng 125(4): 410-416. https://doi.org/10.1061/(asce)0733-9445(1999)125:4(410).

[44] Zeinali Y, Story BA. Impairment localization and quantification using noisy static deformation influence lines and Iterative Multi-parameter Tikhonov Regularization. Mech Syst Signal Pr 2018; 109, 399-419. https://doi.org/10.1016/j.ymssp.2018.02.036.

[45] Chen ZW, Zhao L, Zhang J, Cai Q, Li J, Zhu S. Damage quantification of beam structures using deflection influence line changes and sparse regularization. Adv Struct Eng 2021; 1369433221992482. https://doi.org/10.1177/1369433221992482.